AIAA 79-1697R

Strapdown Attitude Reference Systems: Preliminary Design and Performance Analysis

H. J. Dougherty,* E.J. Pelka,† and J. J. Rodden‡
Lockheed Missiles & Space Company, Inc., Sunnyvale, Calif.

This paper presents a preliminary design approach to strapdown attitude reference system design and performance specification. With equivalent scale factor assumed to be the dominant gyro error source, an iterative technique for gyro and star sensor parameter specification is developed. The star sensor magnitude sensitivity required to yield a star crossing as the star sensor traverses an arbitrary area of the celestial sphere is a central element of the design technique. Attitude reference performance predicted by the method is compared with computer simulation.

Nomenclature

A	= search area between star sensor updates
BW	= gyro bandwidth
M_v	= visual magnitude
P	= probability of at least one star intercept during search
RN	= gyro random noise
SF	= scale factor
t	= time between star sensor updates
β	= gyro input axis misalignment angle
ϵ	= error in scale factor estimate
θ	= maneuver angle about nominal gyro input axis between star sensor updates
$\tilde{\theta}$	= spacecraft pointing or attitude estimate error
$\tilde{\theta}(0)$	= spacecraft pointing error after a star sensor update
λ	= star population density at a given magnitude
ω_G	= spacecraft angular velocity as measured by the gyro
ω_{ref}	= reference angular velocity
ω_v	= true spacecraft angular velocity
$\tilde{\omega}_d$	= error in knowledge of gyro g-insensitive drift
$\mathcal{E}[\ ]$	= expected value operator

Introduction

A DESIGN technique for preliminary performance evaluation and hardware specification for three axis maneuvering spacecraft is presented. Such agile spacecraft attitude reference systems typically consist of three or more strapdown gyros and two or more star epoch (or star crossing) detectors. Coffman[1,2] proposed and analyzed an attitude reference system (ARS) of this type in 1973, and similar systems have been discussed by McAloon et al.,[3] Yong et al.,[4] and Murrell.[5]

During the early stages of a spacecraft's design, an ARS is continually revised and reconfigured. The discontinuous nature of epoch star sensor data complicates ARS performance analysis, and a computer program which adequately simulates the ARS and spacecraft operations can take months to develop. The technique presented in this paper allows an ARS designer to assess the performance of a strapdown system quickly with reasonable accuracy.

The key assumptions upon which the technique is based are as follows: 1) an ARS in which the dominant errors are gyro error sources can be represented as an equivalent scale factor and star sensor errors, and 2) a vehicle effective angular velocity which has a nonzero average value with respect to the stars. The technique applies for any nonzero angular velocities. The technique also applies to cases where the vehicle is arbitrarily commanded to maneuver from one inertially fixed orientation to another.

The design technique does not consider directly two well-known gyro parameters, namely bandwidth and scale factor asymmetry. While a low gyro bandwidth can affect attitude knowledge shortly after maneuver initiation, bandwidth's principal contribution to spacecraft pointing error is associated with control system response. Hence, preliminary bandwidth specification should come from controller analysis. Scale factor asymmetry error for a strapdown gyro is typically on the order of 5-15 ppm, substantially less than the 50-100 ppm scale factor errors considered by the design approach. Both terms should be considered in more detailed analyses.

The discussion describes an applicable gyro model, a star event probability chart, and a procedure by which the ARS designer can select hardware performance parameters. Computer simulation results are presented to demonstrate the effectiveness of the proposed preliminary design technique. The potential extension of the technique to predict the improvement in performance using a Kalman filter or a filter-smoother is also discussed.

Sensor Performance Specification

Figure 1 shows the iterative process that leads to sensor performance specification. Mission objectives and characteristics define an overall spacecraft attitude knowledge requirement and typical spacecraft angular velocity characteristics. These specifications, along with an initial estimate of the gyro parameters, combine to specify an allowable time between star updates and, subsequently, the required star sensor characteristics. The requirements for both gyro and star sensor are then traded to achieve a balance among performance, cost, and reliability. Successive passes through the performance assessment loop verify the adequacy of a parameter set or demonstrate the need for additional trades.

Figure 2 conceptually demonstrates the iterative approach. From the overall mission accuracy required (block A), we subtract the proposed star sensor error and our estimates of gyro drift and random noise induced error. Initially, these

Presented as Paper 79-1697 at the AIAA Guidance and Control Conference, Boulder, Colo., Aug. 6-8, 1979; submitted Oct. 26, 1979; revision received Jan. 16, 1981.

*Manager, Pointing and Control System, Space Telescope Program, Space Systems Division. Member AIAA.

†Staff Engineer, Guidance and Control Systems Department, Space Systems Division. Member AIAA.

‡Manager, Guidance and Control Systems Department, Space Systems Division. Member AIAA.

gyro errors may be set to zero, to yield a scale factor induced pointing error allocation at junction B. Proceeding to curve C we assume a candidate value for equivalent gyro scale factor to establish the allowable maneuver angle between star radiance events. Having established the allowable maneuver angle θ we iteratively branch first to the left (to curves D, E, and F) to reset the allowable gyro drift and noise parameters, an then to the right to reset star sensor parameters (curves G and H). Average spacecraft angular velocity (block A) is used throughout the iterative process. Subtracting the new drift and noise induced pointing errors at junction B yields a new value for allowable attitude error due to gyro scale factor. Again, the gyro error loop can be iterated until the error allocated for scale factor achieves a stable value. Then star sensor parameters can be evaluated. Using the maneuver angle between stars and a candidate value for the star sensor field of view (FOV), the required star sensor sensitivity in terms of star magnitude can be determined.

Gyro Model

Precision gyros are usually rate integrating gyros. The proposed design approach applies equally well to one and two degree-of-freedom gyros. In the case of a two axis gyro, each axis can be treated as a single axis. The dominant gyro errors are scale factor, input axis misalignment, bias, and random noise. Scale factor error sources are composed of linear, nonlinear, asymmetry, stability, and measurement terms. Misalignment can be approximated as an equivalent scale factor error. Scale factor is a maneuver angle dependent error source. Bias and random noise are time dependent errors. Random noise is typically a negligible error contributor. Knowledge of the average rate during the mission effectively makes bias an equivalent scale factor error.

Gyro Error Model

Scale Factor Error

Figure 3 displays gyro output with a linear gyro scale factor. When the slope ω_G/ω_V is 1, the linear scale factor (LSF) error is zero. Typical gyro scale factor errors for precision instruments are less than 0.02%, or 200 ppm. Spacecraft pointing error $\tilde{\theta}$ due to scale factor knowledge error is

$$\tilde{\theta} = \epsilon\theta \tag{1}$$

Equation (1) applies as well to the other types of gyro scale factor error: scale factor stability, scale factor nonlinearity, and scale factor asymmetry. Gyro scale factor nonlinearity represents a deviation in the gyro output from a linear slope. Figure 4 is a conceptual drawing of a gyro's output with the nonlinear scale factor (NLSF) included.

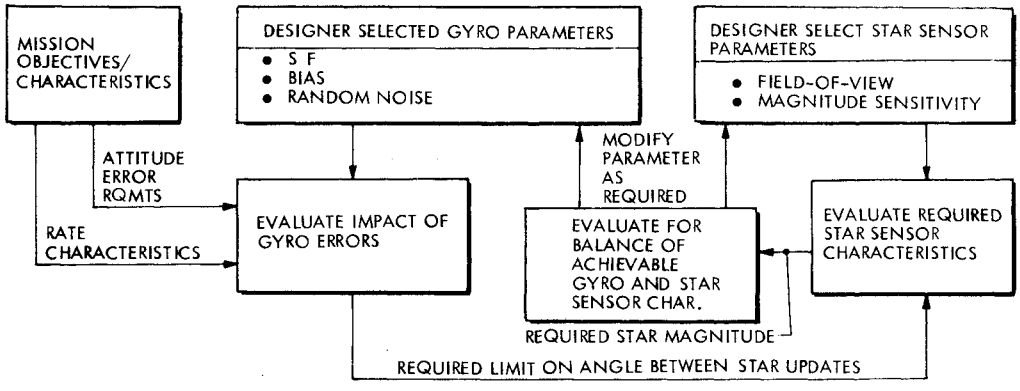

Fig. 1 Instrument performance specification loop.

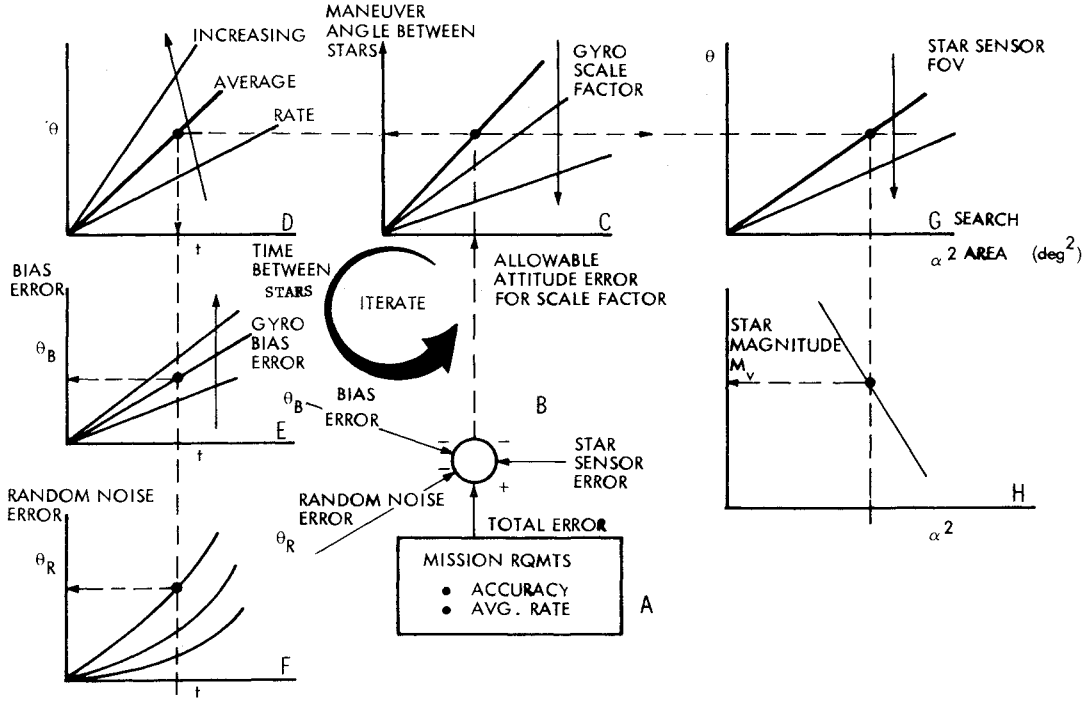

Fig. 2 Iterative design approach.

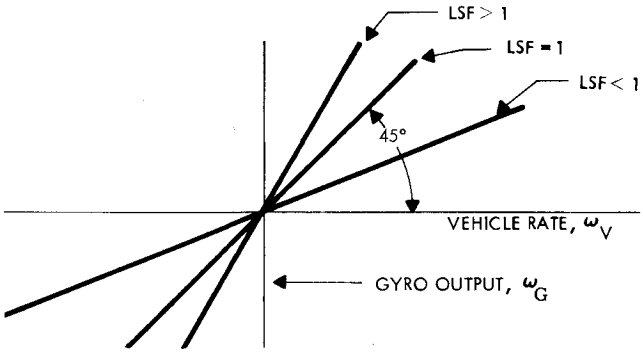

Fig. 3 Gyro linear scale factor.

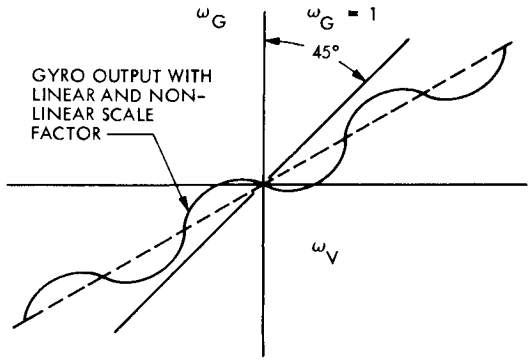

Fig. 4 Representation of gyro output with nonlinear scale factor.

Nonlinear scale factors vary in magnitude as a function of vehicle rate ω_V and are not necessarily periodic functions. As with linear scale factors, the nonlinear error curve can change from gyro to gyro among instruments of the same type. For convenience we use units of deg/h when dealing with nonlinear scale factor. Scale factor errors in deg/h can be converted to ppm as shown in Eq. (2) using a reference angular velocity ω_{ref}. For example, ω_{ref} could be the average spacecraft angular velocity.

$$\text{NLSF(ppm)} = \text{NLSF}\left(\frac{\text{deg}}{\text{h}}\right)\frac{10^6}{\omega_{ref}(\text{deg/s})(3600)} \tag{2}$$

The simplest way to treat NLSF during preliminary design is to include the peak value expected, as an addition to the scale factor ϵ. Scale factor stability and asymmetry can be similarly included.

Curves of constant spacecraft pointing error as a function of slew angle and gyro scale factor error are plotted in Fig. 5. For example, a 100 ppm scale factor error yields a 36 arc-sec spacecraft pointing error after a 100 deg maneuver.

Pointing Errors Resulting from Gyro Input Axis Misalignment

For maneuver angles less than 40 or 50 deg between star updates, the pointing error $\tilde{\theta}$ resulting from gyro input axis misalignment may be approximated as

$$\tilde{\theta} \cong \beta\theta \tag{3}$$

The gyro misalignment angle induced error has the same form as a linear scale factor error and may be treated accordingly; i.e., ϵ may be increased by β.

Gyro Drift-Induced Pointing Errors

Gyro drift-induced pointing error is simply

$$\tilde{\theta} = \tilde{\omega}_d t \tag{4}$$

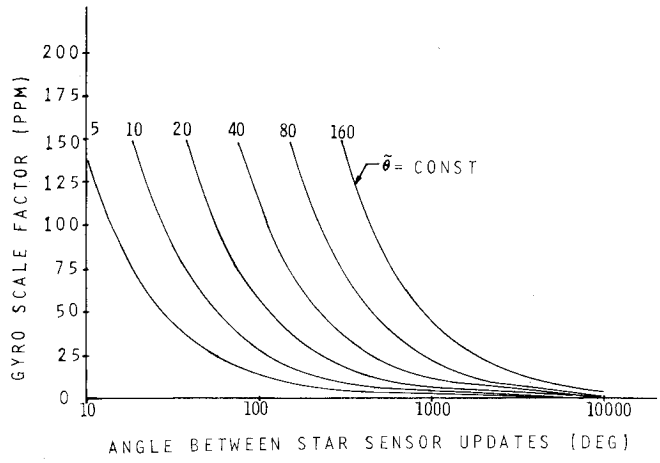

Fig. 5 Curves of constant spacecraft pointing error due to gyro scale factor error.

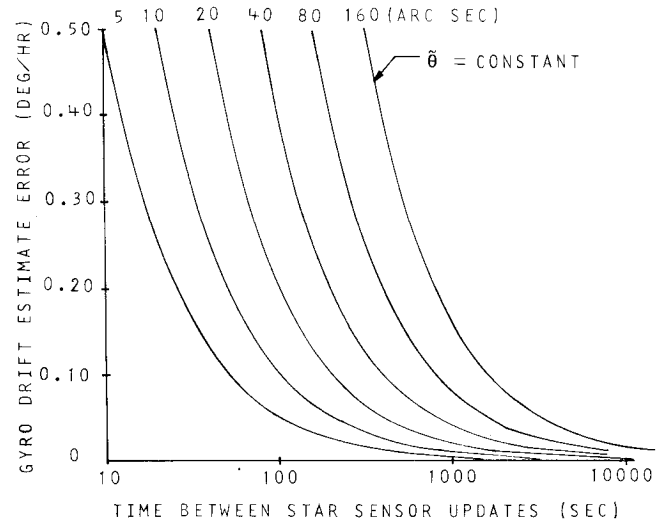

Fig. 6 Curves of constant spacecraft pointing error as a function of gyro drift estimate error.

Drift can be modeled as an equivalent scale factor error of magnitude ω_d/ω_{ref}. For example, a 1 deg/h drift rate and an average spacecraft rate of 1 deg/s results in an equivalent scale factor of 278 ppm. Hence, a precision reference system must have a low drift gyro if the drift effects are to be small, or comparable to that of the actual gyro scale factors. Plots of constant spacecraft pointing error as a function of gyro drift estimate error and time (equivalent to slew angle divided by the average spacecraft rate) are shown in Fig. 6.

Pointing Error Due to Gyro Random Measurement Noise

The random walk Riccati equations for the covariance of the pointing error due to gyro white random measurement noise may be expressed by

$$\frac{\mathrm{d}}{\mathrm{d}t}[\tilde{\theta}^2] = r^2 \tag{5}$$

where

$$r^2 \triangleq \mathcal{E}[\text{RN}^2] \tag{6}$$

The solution for $\tilde{\theta}(t)$ is

$$\tilde{\theta}(t) = [\tilde{\theta}^2(0) + r^2 t]^{1/2} \tag{7}$$

The gyro white noise level r^2 is approximated by the gyro random noise squared, divided by the gyro bandwidth; i.e.,

$$r = [\text{RN}^2/\text{BW}]^{1/2} \tag{8}$$

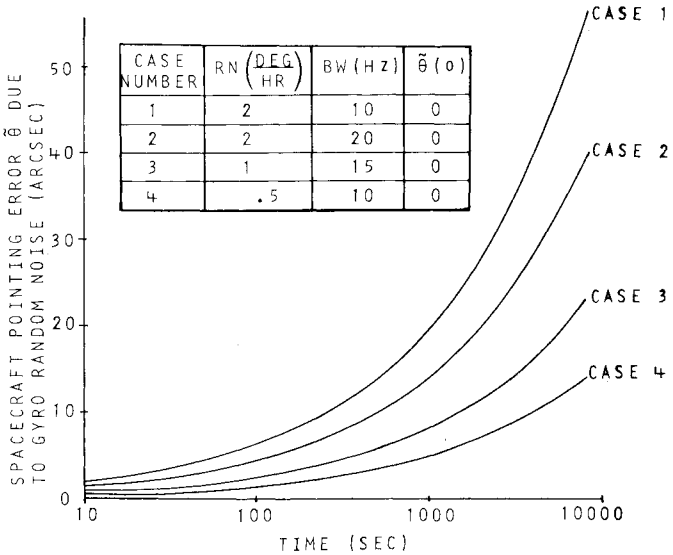

CASE NUMBER	RN (DEG/HR)	BW (HZ)	θ̃ (o)
1	2	10	0
2	2	20	0
3	1	15	0
4	.5	10	0

Fig. 7 Spacecraft random walk pointing error due to gyro random noise.

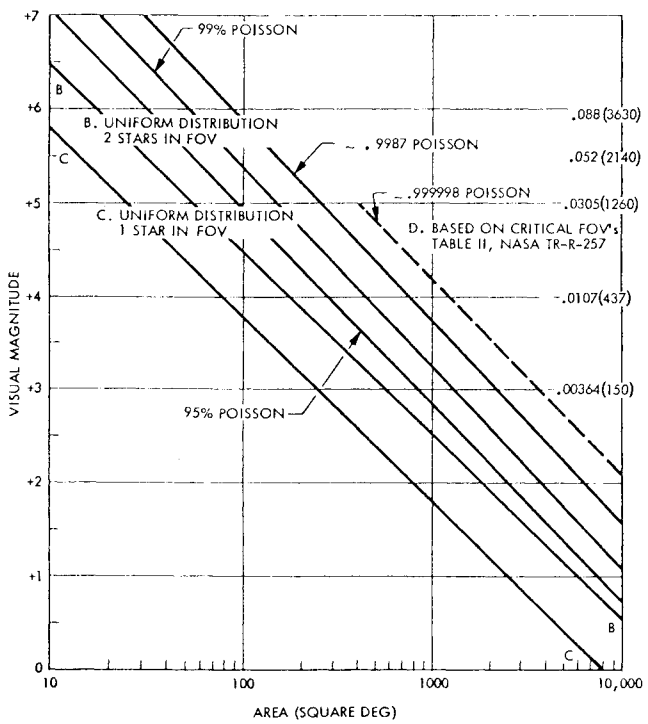

Fig. 8 Search area as a function of visual magnitude.

Time histories of the expected value of the pointing error resulting from gyro random noise are given in Fig. 7.

Star intercepts often occur so frequently that the random noise error contribution to attitude accuracy is negligible.

The Star Chart

The gyro error curves can be used to quickly evaluate single axis attitude determination system accuracy. To use these curves graphically, the star chart shown in Fig. 8 is also needed. The plots represent the probability of a star radiance event as a function of star tracker search area on the celestial sphere and star sensor sensitivity to stellar visual magnitude. The left ordinate is star visual magnitude. The integer numbers marked along the right ordinate in parentheses indicate the number of stars on the sphere at or brighter than the corresponding visual magnitude. The number to the left is the star density in stars/deg^2. For example, there are 150 stars

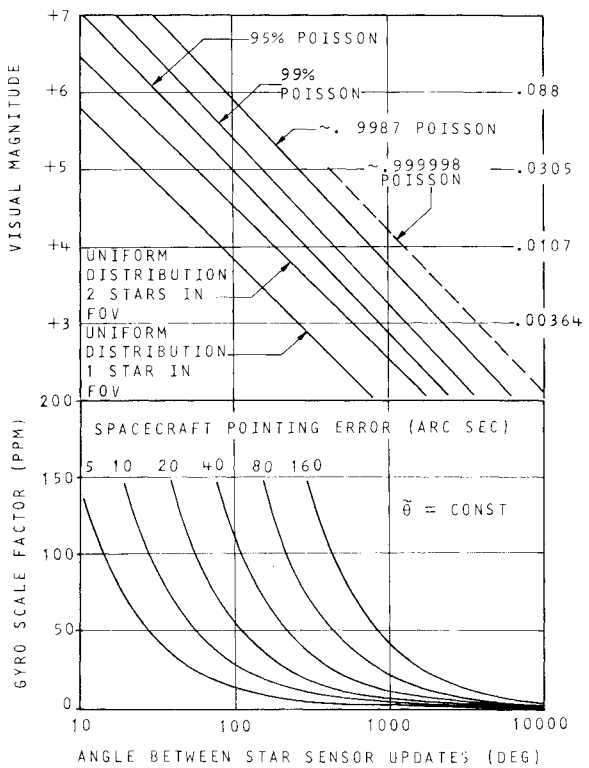

Fig. 9 Example of the star chart overlay to determine pointing error due to a gyro scale factor error.

having visual magnitude +3 or brighter. This means that the corresponding +3 magnitude star density of 0.00364 stars/deg^2. Curves CC and BB of Fig. 8 represent the average area required for a star intercept assuming a uniform distribution of stars over the celestial sphere. To average at least one star intercept for each 100 deg^2 of celestial sphere searched, the star sensor must respond to stars of +3.8 visual magnitude or brighter. In order to average two star intercepts for each 100 deg^2 searched, the star sensor must respond to stars of visual magnitude +4.5 or brighter. The Poisson curves define the star sensor sensitivity required to yield at least one star event for a given area of celestial sphere searched assuming that a radiance event has a Poisson probability distribution with the mean number of stars per square degree. The equation used to define the curves is

$$P = 1 - e^{-\lambda A} \tag{9}$$

The star chart permits trades among field of view, slew angle, and star magnitude.

Using the Star Chart and Gyro Performance Curves to Predict Spacecraft Pointing Errors

The easiest way to explain the use of the charts is by example. Figure 9 shows the star probability chart overlaid onto the scale factor pointing error chart, Fig. 5. The following is a procedure that determines the spacecraft pointing error due to a gyro scale factor error based on Fig. 1: 1) given the ARS accuracy (40 arc-sec, 95% probability), 2) select a gyro scale factor (37.5 ppm), 3) determine the intersection of 37.5 ppm and 40 arc-sec and extend to 95% Poisson curve, and 4) note intersection is at 4 M_v level and corresponds to a 300 deg^2 search area. The designer can select a star sensor FOV based on the 300 deg^2 area. If the first set of gyro and star sensor parameters is not acceptable, the procedure can be repeated with a different parameter set.

The procedure can be extrapolated to obtain an estimate of the accuracy expected if a Kalman filter is used or when post processing of attitude data is performed using a filter-

smoother. This latter category is considered here for often the actual real-time attitude error is not as important as the ability to reconstruct an accurate estimate of attitude after the fact. A heuristic argument may be used to determine likely improvements in performance using both a filter and a filter-smoother. The filter tends to average uncorrelated errors over updates. Since the error propagates between updates, the improvement between two consecutive updates is $\sqrt{2}$. That is, a filter might be expected to have errors about 0.707 that of an unfiltered attitude reference system. The filter-smoother limits the worst case error to half way in angle between updates. Hence, a factor of approximately two additional error reduction might be expected for an overall error of 0.35 that of an unfiltered attitude reference system. Detailed simulation studies varying gyro and star sensor error sources as well as number of stars have shown the preceding values to be good estimates of the average improvement with a filter or filter-smoother. The factor for a filter varied from 0.6 to a value greater than 1. Filter performance can be poorer than that of an unfiltered ARS when the modeled error sources decrease in value to the point where unmodeled sources dominate. An example of a source that does not readily lend itself to modeling is a nonlinear scale factor. The filter-smoother is always better than the unfiltered ARS and the decrease in error varied from 0.1 to 0.7. Again, the larger factors occur when unmodeled sources dominate. In general, the larger the error due to modeled error sources, the more improvement a filter or filter-smoother offers. Hence, in any performance study, the relative values of modeled and unmodeled error contribution should be compared to allow an estimate of expected performance improvements with a filter or filter-smoother. Also, while increasing the number of stars improves performance, the improvement is slightly above 1000 stars. The biggest improvement is in going from an unfiltered or filtered ARS to a filter-smoother.

Table 1 Instrument error magnitudes for performance comparison test

Error source	Error magnitude
Gyro misalignment angle magnitude, arc-sec	30
Gyro nonlinear scale factor error, deg/h	0.25
Gyro linear scale factor estimate error, ppm	28.3
Gyro linear scale factor drift error, ppm	28.3
Gyro g-insensitive drift estimate error, deg/h	0.10
Star sensor field-of-view, deg	6
Star sensor misalignment, arc-sec	20
Star sensor random measurement noise, arc-sec	20
Dimmest stars observable (vis mag)	4

Table 2 Single axis maneuver pointing error summary

Error source	Contribution to single axis pointing error, arc-sec
Gyro misalignment	25.0
Nonlinear scale factor	25.0
Linear scale factor estimator error	5.1
Linear scale factor drift induced error	5.1
g-insensitive drift	10
Star sensor random noise	20
Star sensor alignment estimate error	20
Rss	47.6

Example of System Performance Comparison

The ability of the described technique to estimate attitude reference system performance is illustrated by several detailed examples. The examples are based on specific maneuver profiles to illustrate how accurately the technique can predict results. In actual practice, the technique can be used to estimate performance prior to the detailed simulation.

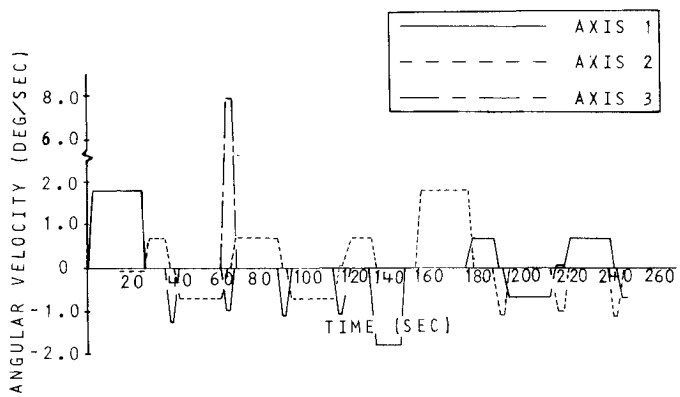

Fig. 10 Spacecraft angular velocity profile.

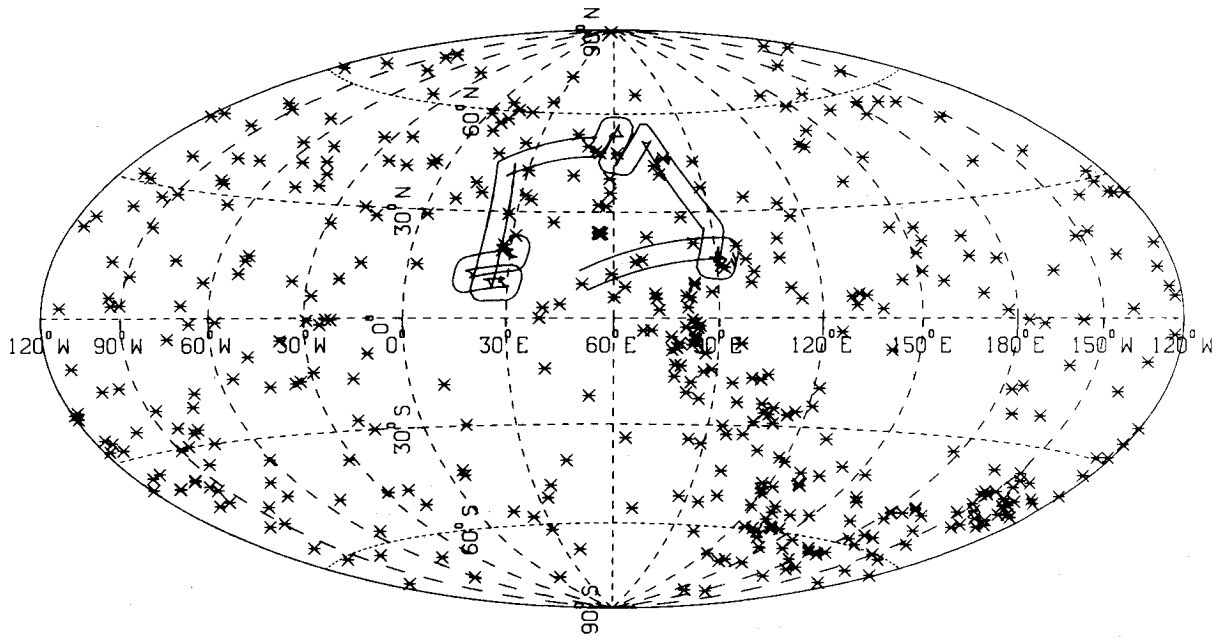

Fig. 11 Typical projection of star sensor field-of-view onto celestial sphere during performance comparison test.

Example: The spacecraft model has three star sensors with 6 deg FOV and two slits per FOV.§ The sensor detects fourth-M_v stars. The gyro and star sensor errors are as shown in Table 1 and the x, y, and z axis average rates are 0.5, 0.5, and 0.17 deg/s, respectively, for 253 s. The 95% probability estimate of attitude error is determined as follows:

1) The equivalent scale factor error for nonlinear scale factor and gyro misalignment are determined from Eqs. (2) and (3) to be 139 and 145 ppm, respectively. The total scale factor error ϵ is 205 ppm (rss), including scale factor linearity and stability.

2) The M_v four, 95% star probability curve indicates a 300 deg^2 search of the celestial sphere for at least one star, yielding at 50 deg maneuver between star intercepts for 6 deg star sensor FOV.

3) The 95% probability error due to gyro scale factor (SF) error is given by the relationship:

$$\text{SF error} = (\text{gyro SF}) \times \begin{pmatrix}\text{95\% probability maneuver angle} \\ \text{between star intercepts}\end{pmatrix}$$
$$= (205 \times 10^{-6}) \times (50 \text{ deg}) \times 3600 \text{ arc-sec/deg}$$
$$= 37 \text{ arc-sec}$$

The individual contribution by each scale factor source is determined as the preceding and is summarized in Table 2.

3) The time-dependent errors, e.g., gyro bias, can be estimated as follows:

$$\text{bias error} = \frac{(\text{gyro bias})}{(\text{average rate})} \times \begin{pmatrix}\text{95\% maneuver angle between} \\ \text{star intercepts}\end{pmatrix}$$

The x, y, and z errors are 10, 10, and 29 arc-sec, respectively.

4) The single-axis error is determined by root sum squaring the gyro and star sensor errors and is 48 arc-sec for x and y, and 55 arc-sec for z. The x and y axes contributors are shown in Table 2.

5) The *average* number of star intercepts as determined from a uniform distribution and is given by:

$$\text{avg. no. stars} = (\text{star density}) \times (\text{total maneuver angle}) \times (\text{FOV}) \times (\text{no. sensors}) \times (\text{no. slits per sensor})$$
$$= (0.0107)\sqrt{(5)^2 \times (0.5)^2 \times (0.17)^2} \times 253 \times 6 \times 3 \times 2$$
$$= 70 \text{ stars}$$

Consider the specific maneuver profile shown in Fig. 10 which satisfies the conditions in the preceding example. For the total simulation, spacecraft x axis (axis 1) angular velocity and y axis (axis 2) angular velocity each have an average magnitude equal to 0.5 deg/s. A single, high rate, 42 deg z axis (axis 3) maneuver occurred 65 s after the run was initiated.

§Star scanners require a star to traverse the slit in order to provide a radiance signal. They do not respond to a star located along the scanner boresight. Furthermore, a single radiance event, from an unlabeled slit, provides little information relative to spacecraft attitude about the scanner boresight axis. Hence, a scanner with k nonparallel slits each extending across the complete sensor field-of-view is modeled to have two orthogonal slits, both normal to the sensor boresight.

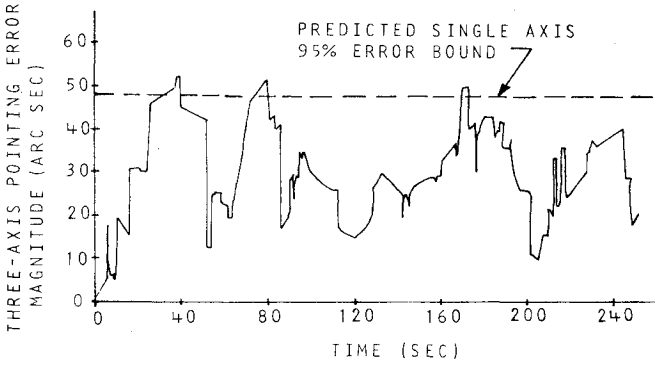

Fig. 12 Time history of computer simulation generated three axis pointing error magnitude for comparison test.

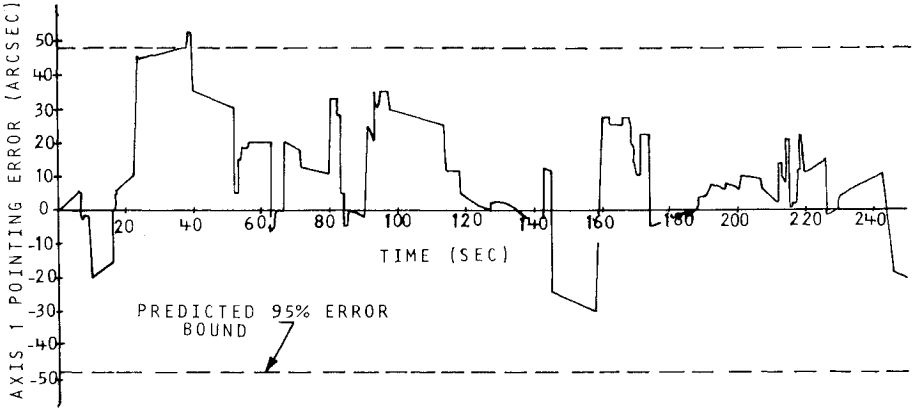

Fig. 13 Axis 1 pointing error time history for comparison test.

Table 3 Test case results summary

	Comparison test	Intermediate error test	Small error test	Modified orbit error test	10 deg FOV test
Calculated 95% error level,[a] arc-sec	48	21	8.9	8.0	34
Simulation 95% error level,[b] arc-sec	49	22	8.3	9.6	36
Number of stars occurring simulation	95	95	95	58	50
Average angular velocity, deg/s	0.50	0.50	0.50	0.50	1.00
Deviation in 95% error level, %	2.0	4.5	−7.2	7.3	5.6

[a] Single axis error estimate.
[b] Vector error.

Table 4 Error magnitude for test case 2—intermediate error magnitudes

Error source	Error magnitude	Contribution to spacecraft pointing error, arc-sec
Gyro misalignment angle magnitude, arc-sec	5.0	4.40
Gyro nonlinear scale factor error, deg/h	0.12	12.00
Gyro linear scale factor estimate error, ppm	28.3	5.04
Gyro linear scale factor drift error, ppm	28.3	5.04
Gyro g-insensitive drift estimate error, deg/h	0.10	10.00
Star sensor misalignment, arc-sec	6.00	6.00
Star sensor random measurement noise, arc-sec	10.0	10.0
Rss, arc-sec	...	21

Table 5 Error magnitudes for test case—small error magnitudes

Error source	Error magnitude	Contribution to spacecraft pointing error, arc-sec
Gyro nonlinear scale factor error, deg/h	0.01	1.00
Gyro linear scale factor estimate error, ppm	28.3	5.04
Gyro linear scale factor drift error, ppm	28.3	5.04
Gyro g-insensitive drift estimate error, deg/h	0.05	5.00
Star sensor random measurement noise, arc-sec	2.00	2.00
Rss, arc-sec	...	8.9

Figure 11 displays a typical projection of one star sensor's field-of-view onto the celestial sphere during the simulation run. The small stars or crosses in the figures are star positions.

Star sensors 1, 2, and 3 detected 9, 9, and 14 distinct (or separate) stars, respectively, as shown in the figure. The entire star sensor system recorded 95 star intercepts. This compares with 70 intercepts predicted by a simple area calculation using two crossing slits per sensor.

A time history of the spacecraft three-axis pointing error appears in Fig. 12. The worst-case pointing error occurred at 39 s and had a magnitude of approximately 54 arc-sec. Ninety-five percent of all pointing errors were less than 49 arc-sec. The x axis (axis 1) pointing error time history appears in Fig. 13. Axis 1 worst-case pointing was 53 arc-sec at 39 s. Traces of axis 2 and axis 3 pointing error were similar to the axis 1 trace, with worst cases being -40 arc-sec (at 188 s) and -43 arc-sec (at 80 s), respectively.

Comparison of the computer simulation results with the preliminary pointing estimate shows that 1) single-axis estimation is representative of the single-axis error; 2) total vector error is less than the rss of the estimated single axis error sources; and 3) estimated average number of stars was less than that observed in the simulation. The x and y error estimates of error agree well with the simulation. The z axis error estimate tends to be high due to the fact only one maneuver occurred in the interval. Hence, the z gyro error was dominantly bias. The rss vector estimate of the single axis 95% errors can be expected to exceed the vector 95% error since the 95% single axis errors do not occur simultaneously. Hence, the rss of the estimated errors gives a conservative value of ARS performance. The calculated average number of stars is usually less than the actual number of intercepts due to the fact that the Poisson estimate of star statistics falls below actual catalog statistics for multiple star encounters, while it is a good estimate of at least one intercept.

Table 6 Error magnitude for test case 5—star sensor FOV set 10 deg

Error source	Error magnitude	Contribution to spacecraft pointing error, arc-sec
Gyro misalignment angle magnitude, arc-sec	30.00	15.7
Gyro nonlinear scale factor error, deg/h	0.25	7.5
Gyro linear scale factor estimate error, ppm	28.3	3.1
Gyro linear scale factor drift error, ppm	28.3	3.1
Gyro g-insensitive drift estimate error, deg/h	0.10	3
Gyro bandwidth, Hz	10.00	...
Star sensor misalignment, arc-sec	20.00	20
Star sensor random measurement noise, arc-sec	20.00	20
Rss, arc-sec	...	34

To demonstrate the correlation between the graphical design technique and three axis simulation, Table 3 lists numerical results for the test described earlier and four additional cases. The first row of Table 3 lists the pointing error for each case as predicted by the graphical technique. Row 2 provides the actual 95% simulation response for each case. The last row of Table 3 lists the percentage deviation between the graphically predicted 95% pointing error (row 1) and computer simulation results (row 2). Column 1, labeled "Comparison test," lists the results for the simulation just discussed. Columns 2 and 3 list results for test cases in which gyro and star sensor error magnitudes were changed, but the orbit and maneuver sequence remained that of the column 1 comparison test case. Instrument error data for these cases appear in Tables 4 and 5. The modified orbit error test used the same instrument errors and maneuver sequence as did the column 3 test. For this case the spacecraft initial orientation was rotated with respect to the celestial sphere to demonstrate the effects of different star fields on system performance. Finally, the 10 deg FOV test was included to demonstrate the effects of widening the star sensor field-of-view. Instrument errors and spacecraft initial orientation were the same as for the original comparison test. Test case error magnitudes along with predicted vehicle pointing errors appear in Table 6. The results listed in Table 3 demonstrate agreement between the design technique and computer simulation to approximately 10%.

To demonstrate the improvement with a Kalman filter and a filter-smoother, the attitude error for an ARS with 50 ppm linear scale factor, 55 ppm scale factor nonlinearity, and 0.1 deg/h bias is calculated. The average rate in the x and y axes is approximately 1.2 deg/s. The rms results are calculated for 440 and 1300 stars. The filter and filter-smoother estimated only attitude, linear scale factor, and bias. The estimates using the proposed technique are compared with simulation results.

1) The equivalent scale factor due to bias is $(0.1)(1/3600)(1.2)\ 10^6 - 23$ ppm in x and y. The rss of the equivalent bias scale factor and the linear scale factor is approximately 55 ppm. This value is comparable to that for the nonlinear scale factor. Since the nonlinear scale factor is unmodeled in the filter, we expect the filter and filter-smoother improvements will be at best comparable to the average improvement values 0.7 and 0.35, respectively. The rss of the scale factor values is approximately 78 ppm.

2) For an rms (i.e., probability of 0.68, attitude error estimate) the area A as determined from Eq. (9) for 440 and

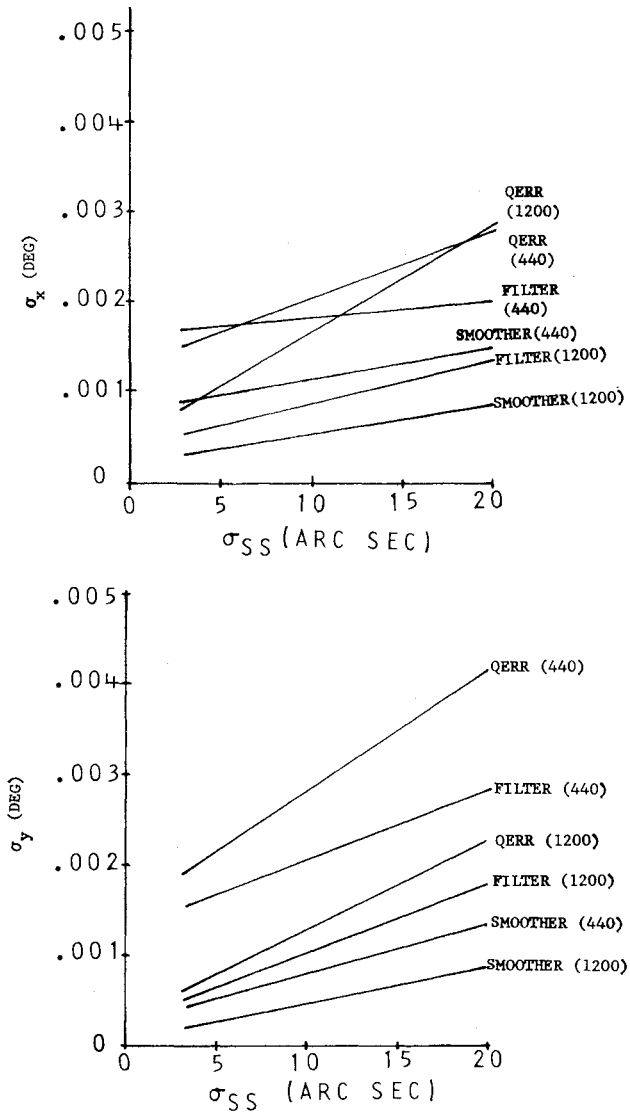

Fig. 14 Comparison of unfiltered, filtered, and smoothed ARS.

1300 stars is 107 and 36 deg^2, respectively. For a 6 deg FOV, the associated maneuver angle for at least one star is 17.8 and 6 deg, respectively.

3) Single axis rms error due to equivalent scale factor for 440 and 1300 stars is 0.0014 and 0.0005 deg, respectively.

4) The total estimate of the rms error is obtained by root sum squaring the gyro and star sensor errors. Assuming θ = star sensor error of 5 arc-sec (rms), the error for 440 and 1300 stars is 0.002 and 0.0015 deg, respectively.

5) The improvement expected from a filter and filter-smoother is at best approximately 0.7 and 0.35 due to the large value of nonlinear scale factor.

Figure 14 illustrates the results of the simulation with single axis error plotted as a function of star sensor measurement noise θ_{ss} with both type of ARS and number of stars as parameters. The x axis errors agree with the unfiltered ARS predictions. The y-axis results are about 40% higher for 440 stars and compare favorably for the 1300 star case. As the star sensor error decreases, the unfiltered estimate tends to give upper bounds on the error. The filter and filter-smoother improvement relative to an unfiltered ARS varies from 0.5 to 1 and 0.3 to 0.7, respectively. The associated average values are approximately 0.7 and 0.5, respectively. In the x axis, the filter results for 440 stars at low star sensor errors does slightly poorer than the unfiltered ARS. This result and the modest improvement using the filter and filter-smoother is due to the relatively large unmodeled error.

Conclusion

The preliminary design approach for the attitude reference system leads to conservative estimates for the vector error when the root sum square of the three single-axis estimates is used to predict vector error. This is often a prudent approach in a preliminary design. As the mission objectives and requirements become better defined, the single axis estimate provides values to within 10% of simulation results. The speed with which an attitude reference system can be sized with the proposed approach allows rapid trade of mission performance and hardware parameters.

Acknowledgments

The authors wish to express their appreciation to Santos Torres, who provided the computer simulation results, and to Pearl Clark who typed the manuscripts for this paper.

References

[1] Coffman, V.D. and DeBra, D.B., "Estimation of Gyro Parameters for Experimentally Developed Gyro Models," AIAA Paper 75-1071, AIAA Guidance and Control Conference, Boston, Mass., Aug. 20-22, 1975.

[2] Coffman, V.D., "On-Line Estimation of Parameters Using Experimentally Developed Gyro Models, and Other Applications," Dept. of Aeronautics and Astronautics, Stanford Univ., Stanford, Calif., SUNDAR No. 467, Dec. 1973.

[3] McAloon, K.J., Farrenkopf, R.L., Balsky, F.J., and Mann, R.J., "Performance Tests of Two Precision Attitude Determination Systems," AIAA Paper 77-1039, AIAA Guidance and Control Conference, Hollywood, Fla., Aug. 8-10, 1977.

[4] Yong, K. and Headley, R.P., "Real Time Precision Attitude Determination System (RETPAD) For Highly Maneuverable Spacecrafts," AIAA Paper 78-1246, AIAA Guidance and Control Conference, Palo Alto, Calif., Aug. 7-9, 1978.

[5] Murrell, J.W., "Precision Attitude Determination For Multimission Spacecraft," AIAA Paper 78-1248, AIAA Guidance and Control Conference, Palo Alto, Calif., Aug. 7-9, 1978.